celc.202100609.R1: 09/07/2021

Decorating BODIPY with electron-withdrawing NO group: spectroelectrochemical consequences and computational investigation

Thaissa Lucio Silva[1,2], Tamires Alves do Nascimento[1], Andresa K. A. de Almeida[1], Shaiani M. G. Melo[3], Julio C. S. Da Silva[1], Jadriane Almeida Xavier[1], André Felipe de Almeida Xavier, Danyelle Cândido Santos[1], Jay Wadhawan[4], Flavio S. Emery[3], Marilia O. F. Goulart[1*]

[1]Instituto de Química e Biotecnologia, Universidade Federal de Alagoas, Maceió, Alagoas, 57072970.
[2]Núcleo de Ciências Exatas - NCEx, Universidade Federal de Alagoas, *Campus* de Arapiraca, Arapiraca - AL, CEP: 57309-005, Brasil.
[3]Departamento de Ciências Farmacêuticas, Faculdade de Ciências Farmacêuticas de Ribeirão Preto, Universidade de São Paulo, Ribeirão Preto, SP, Brazil.
[4] Hull University, Department of Chemical Engineering, Cottingham Road, Hull HU6 7RX, United Kingdom.

Correspondence to:

Prof. Marília Oliveira Fonseca Goulart: Campus A. C. Simões, Avenida Lourival Melo Mota, s/n, Tabuleiro dos Martins, 57072-970 Maceió, AL, Brazil; +55 (82) 98818 – 0463
mofg@qui.ufal.br

Thaissa Lucio Silva and Tamires Alves do Nascimento contributed equally to this work.

Graphical Abstract

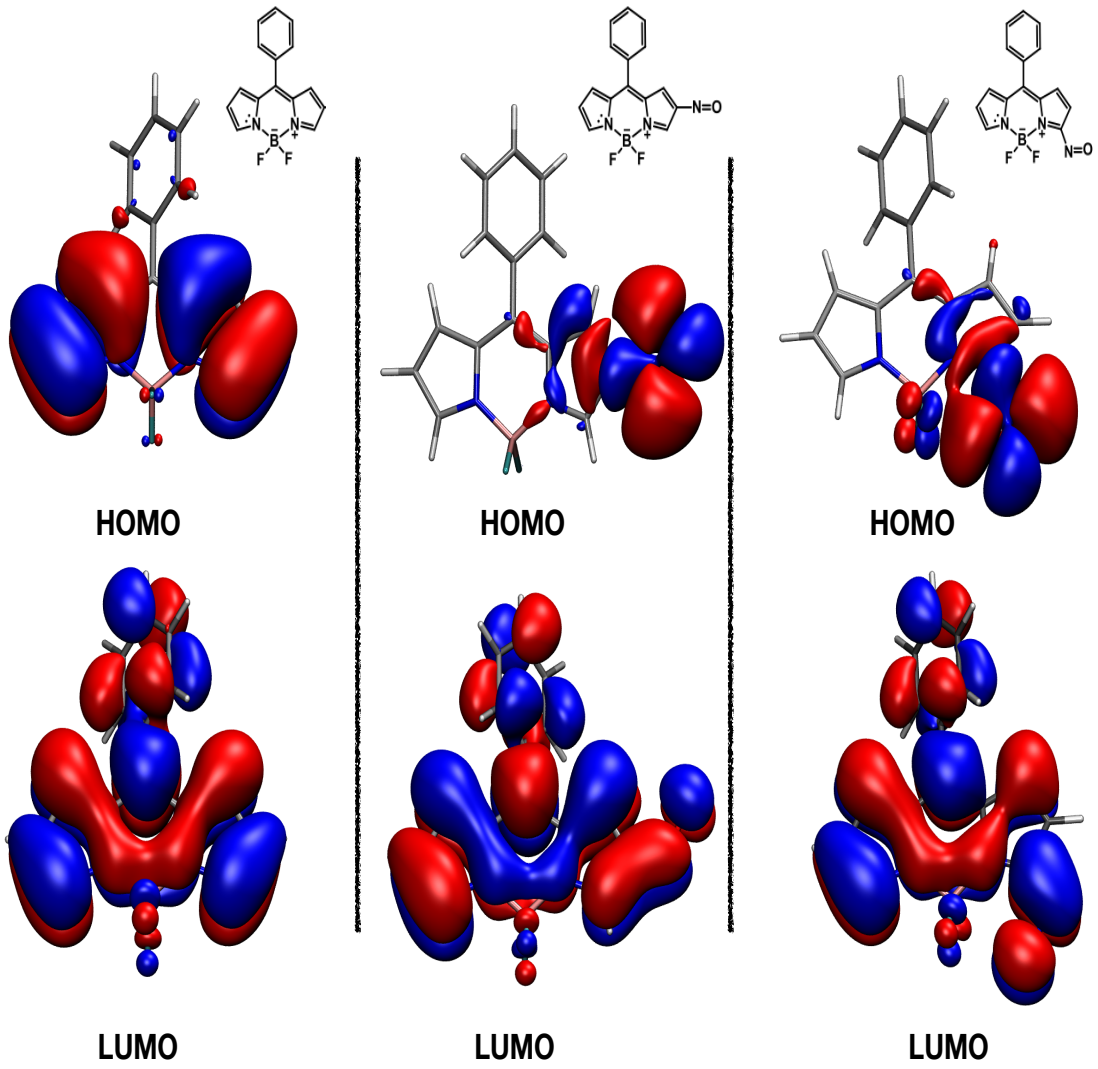

HIGHLIGHTS

Positional isomers (α or β) of nitrosyl-BODIPY exhibit contracting molecular reactivities.

Solvent-influenced, reversible dimer formation of the nitrosyl-BODIPYs is significant.

Spectroelectrochemistry coupled with CDFT analysis explain the unexpected reactivity differences.

The nitrosyl group is the first to be reduced in the 5-nitrosyl-BODIPY.

For the 6-nitrosyl-BODIPY, the nitrosyl group strongly facilitates the reduction, which occurs in the BODIPY core.

The –NO group on the BODIPY core is the one to be first oxidized, independent on the position in the ring.

ABSTRACT: 4,4-difluoro-5,7-dimethyl-4-bora-3a,4a-diaza-s-indacene (BODIPY) and derivatives are an outstanding class of fluorescent dyes, We, herein, report the effect of the introduction of a nitrosyl moiety into the BODIPY structure and its dramatic effect on the observed electrochemical reaction mechanism. 6-Nitrosyl-8-phenyl-BODIPY and its 5-nitrosyl positional isomer, compounds **2** and **3** , respectively, were obtained from the *meso* precursor, 8-phenyl-BODIPY (**1**), by nitrosation. Electrochemical studies for **1** - **3** are reported. Cyclic voltammetry and differential pulse voltammetry, in degassed DMF or in MeCN (reduction + oxidation), both with *n* -Bu_4NPF_6 (0.1 M), were obtained. Compound **1** displays the usual behaviour for 8-phenyl substituted BODIPYs. The addition of the acceptor nitroso group, in compounds **2** (in position β) and **3** (in position α), leads to a different profile. For all the compounds, the nitroso group greatly facilitates the reductions. For compound **3** ($E_{pIc/2}$ = -0.238 V), the first to be reduced is the nitroso group, due to the stability of the electrogenerated radical anion, along with non-bonding interactions with the electronegative boron difluoride, differently from compound **2** ($E_{pIc/2}$ = -0.351 V), with a β-nitroso group, where the nitroso-based facilitated reduction occurs in the substituted BODIPY core. Spectroelectrochemistry coupled with analysis through Conceptual Density Functional Theory (CDFT) corroborate the voltammetric results, and explain the unexpected reactivity differences.

Keywords: electroreduction, electrooxidation, substituent effects, electrodic mechanisms, weak interactions

1. INTRODUCTION

Small fluorescent molecules enable the precise interrogation of clinical, biomedical, and environmental sciences [1]. Among the available classes of fluorescent dyes, our group is interested in BODIPYs (acronym for 4,4-difluoro-5,7-dimethyl-4-bora-3a,4a-diaza-s-indacene), first reported by Treibs and Kreuzer in 1969 [2].

BODIPY has three π-delocalized rings: a pyrrole, an azafulvene and a diazaborinin-type system, which, in the parent compound, exist as two equivalent resonance forms, which cannot be distinguished [3]. The dipyrrin chelation to a difluoroboryl unit restricts molecular flexibility, acting as a bridge, leads to outstanding photophysical properties, including high fluorescence quantum yields, sharp emission and absorption peaks, and high molar absorptivity [4]. Along with their excellent thermal and photochemical stabilities, good solubility, chemical robustness, and versatility, their properties can be easily modulated by pre- or post-functionalizations, which can fine-tune their rich redox and photophysical properties [4,5].

The use of BODIPY-based compounds relies upon a thorough understanding of their electronic properties. Extensive studies have been performed on BODIPY and its analogues to evaluate and understand their optical and electronic properties [3-5]. Additional conjugation can modify absorption and emission spectra, leading to different applications. Within this context, the most effective strategy to tune fluorescence is based on the development of dyads in which an internal electron transfer or an energy transfer between a redox-active system and a fluorescent core can be enabled or suppressed [5].

However, it is important to emphasize that introducing new functional groups is not without challenges, especially in cases where additional molecular asymmetry is introduced [6]. Recently, nitrosyl monosubstitution of BODIPYs was reported in the literature [7], and this direct nitrosation opens up several avenues for the development of new fluorescent probes, for different applications. These monosubstituted BODIPY derivatives are asymmetric

around the difluoroboron-dipyrromethene ring, so that they may be represented by resonance forms, whose contributions in the pyrrole and azafulvene rings might be different, one being dominant over the others. Consequently, it is very important to know the different electronic structures and the intensity of their aromatic character, for understanding their redox reactivity. Accordingly, computational structure analysis reveals that the aromaticity is affected whenever electron-donating groups (EDG) and electron-withdrawing ones (EWG) are present as substituents in the α and β positions of the BODIPY core. Generally, dominant resonance structures for EWG-substituted BODIPYs have a more aromatic character [3]. Delocalization of the non-bonding electrons for a 3-phenylamino substituted BODIPY chromophore has been described, together with an hydrogen bond existing in a six-ring between the aromatic NH and one of the out-of-plane fluoride groups attached to boron [8].

This paper is concerned with the electrochemical reactivity of asymmetric, monosubstituted nitrosyl positional isomers of 8-substituted phenyl BODIPY compounds, compared with the unsubstituted parent (compound **1**, Figure 1). In the two isomers considered, 6-nitrosyl-8-phenyl-BODIPY (compound **2**) and 5-nitrosyl-8-phenyl-BODIPY (compound **3**) [7], the dominant canonical structures in the neutral form are aromatic: the substitution occurs on the pyrrole ring, depicted in Figure 1.

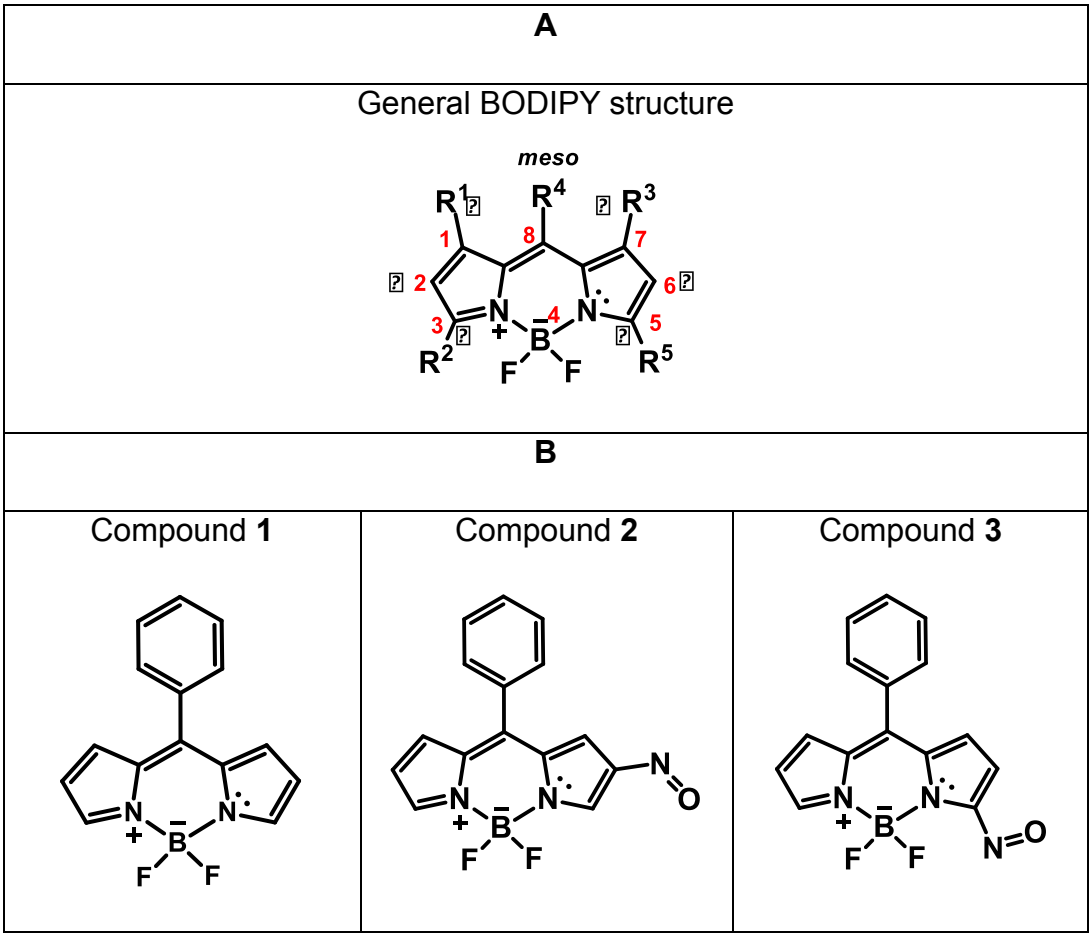

Figure 1. Structures of BODIPY core (**A**) and derivatives investigated, showing the main canonical resonance forms (**B**).

An interesting feature of most BODIPY dyes is that the main structural framework undergoes reversible oxidation and reduction processes at accessible potentials [8-10]. Electrochemical studies are useful in understanding the redox properties of these materials and in evaluating structure stability relations for the radical ions, cation or anion ones [11-12]. Coupled with spectroscopic measurements, these studies help researchers in the design of novel compounds with specific properties [4-6, 8, 11-12].

Reports on the electrochemistry of BODIPYs are relatively new [13-23] and have been gaining importance recently, due to the possibility of application in electrogenerated chemiluminescence. Their electrochemical properties are very much dependent on experimental conditions and their chemical structures, especially in terms of substitution at the *meso* (or 8-position) (R^4), α (or 3- and 5-positions) (R^2 or R^5) and β (or 1-, 2-, 6-, or 7-) positions (R^1 or R^3) (Figure 1A). Indeed, in case of fully substituted species, reversible Nernstian one-electron

oxidation and reduction occur, generating highly stable radical anions or radical cations; in contrast, in the absence of substitution, the electrogenerated intermediates are more reactive and prone to suffer additional chemical reactions. In general, compared with aromatic hydrocarbons, BODIPY derivatives are relatively easy to reduce, with the second electron reduction being thermodynamically more difficult. Surprisingly, however, the large majority of previous electrochemical investigations of BODIPY dyes have only been concerned with the first oxidation and reduction waves [13,16]. Likewise, the reduced form of BODIPY species has not been characterized extensively [12]. Yet such studies are particularly relevant when considering the use of BODIPY moieties in strongly reducing conditions, including biological anoxic environments [12], as they may be able to unravel both qualitative and quantitative insights into the observed behaviour of the BODIPY species.

The electrochemistry of nitrosoarenes had been extensively studied by CV in aprotic solvents, such as MeCN, DMF or DMSO [24-26], primarily as a result of their participation as an intermediate during the reduction of nitroaromatic reduction, together with their application as spin traps. Aromatic *C*-nitroso compounds are known to exist as free monomers in equilibrium with *cis*- or *trans*- azodioxy (-($^{-}$O)N^{+}=$^{+}$N(O^{-})-) dimers in solution, with consequences for their electrochemical behaviour. However, the effect of the bathing solvent medium is known to play an important role in the dimerization [25], which is thought to result from dipole-dipole interactions [25], since the *cis*-isomer has a large net dipole, whilst the *trans*-isomer may retain a weak net dipole.

Herein, we describe the investigation of the three compounds (**1-3**). We are particularly interested in analyzing the effects of the location of the nitrosyl group on the electrochemical reactivity and stability, as this may influence their applications for, for example, *in vivo* assays. Whilst a number of authors typically have used CH_2Cl_2 as the polar, aprotic solvent for the electrochemical analysis, we report studies in *N*,*N*-dimethylformamide (DMF) and acetonitrile (MeCN), since these can be used during *in vitro* tests. These two solvents have similar dielectric constants, and also enable a good solubility of the BODIPY compounds.

2. EXPERIMENTAL PART

*2.1 Synthesis of compounds **1**, **2**, and **3**.*

The synthesis and characterization of the compounds **1**-**3** were recently reported [7] and the purity of the compounds was verified by HRMS, elemental analysis and by obtention of mixed melting points (m.p). with authentical samples [7].

2.2 Electrochemical Studies.

2.2.1 Cyclic Voltammetry (CV):

Cyclic voltammetry (CV) experiments were performed with a conventional three-electrode cell in an Autolab PGSTAT-30 potentiostat (Echo Chemie, Utrecht, The Netherlands) coupled to a PC microcomputer, using GPES 4.9 software. The working electrode was a glassy carbon (GC, BAS, d = 3 mm), the counter electrode was a Pt wire, with an Ag|AgCl|Cl^- (saturated) reference electrode. All electrodes were contained in a one-compartment electrochemical cell with a volumetric capacity of 5 mL. The GC electrode was cleaned up by polishing with alumina on a polishing felt (BAS polishing kit). The solvents used in aprotic media studies were extra dry DMF (99.8%) acquired from Acros Organics and MeCN, purchased from Acros Organics (99.9%, extra dry, over molecular sieves, AcroSeal®). The supporting electrolyte was tetra-*n*-butylammonium hexafluorophosphate ($TBAPF_6$), which was used as received from Sigma Aldrich (St. Louis, USA). In CV experiments, electrochemical reduction was performed in aprotic media (DMF or MeCN + 0.1 mol L^{-1} $TBAPF_6$). Each compound (1 x 10^{-3} mol L^{-1}) was added to the supporting electrolyte. For reduction studies, it was necessary to degas the cell with a flux of argon that was kept over the solution for the experiments [27]. In DMF, due to the presence of an oxidation peak (around +1.2 V vs Ag|AgCl|Cl^- (saturated)), from the supporting electrolyte in the anodic region, it was not possible to analyse the oxidation profile (Fig. S1). This analysis was conducted in MeCN. For electrochemical investigations in MeCN, the same concentration of the compounds (1 x 10^{-3} mol L^{-1}) was used. As with DMF studies, the cell was degassed with an argon flow with an argon blanket over the solution during the experiments. After the experiments, ferrocene, acquired from Sigma Aldrich

(98%) (St. Louis, USA), with the same concentration of the compounds (1 x 10^{-3} mol L^{-1}) was added as an internal standard. The cyclic voltammograms related to Fc/Fc^{+} are shown in Supplementary Information (Figs. S2-S4, Table S1), in comparison to the ones, obtained versus $Ag|AgCl|Cl^{-}$ (saturated) reference electrode (Figs. S5-S7, Table S2). In the CV experiments, the scan rate was varied in the range 35 to 500 mV s^{-1}. All experiments were performed at room temperature (25 $\pm$ 2 ^{o}C).

2.2.2 Spectroelectrochemical experiments:

These were performed on a thin-layer quartz electrochemical cell (path length 1 mm, BASi) with a three-electrode arrangement consisting of an optically transparent Pt minigrid as working electrode, a Pt wire as counter electrode and a $Ag|AgCl|Cl^{-}$ (saturated) reference electrode. The cell was paired to the already described potentiostat, and the spectra were obtained using a Hewlett Packard 8453 spectrophotometer [27]. Measurements were carried out on deoxygenated solutions in DMF + $TBAPF_6$ 0.1 mol L^{-1}, at room temperature. The concentrations of compounds **1**-**3** were 2.5 x 10^{-3} mol L^{-1}. The applied potentials were -1.00 V and -1.60 V (compound **1**), -0.35 V, -1.40 V, -1.70 V (compound **2**) and -0.25 V, -1.00 V (compound **3**). The measurements in MeCN + $TBAPF_6$ 0.1 mol L^{-1}, as well as in DMF, were at room temperature (25 $\pm$ 2 ^{o}C), in the same concentrations mentioned above (compounds **1** and **3** were 2.5 x 10^{-3} mol L^{-1}). The applied potentials were -1.00 V, -1.60 V and +1.30 V (compound **1**) and -0.25 V, -1.00 V (compound **3**).

2.2.3 Computational Details:

Full unconstrained geometry optimization and frequency calculations were carried out using density functional theory with the hybrid GGA B3LYP exchange-correlation [28-29] including the D2 dispersion correction proposed by Grimme [29]. All the atoms were described using the 6-311G(d,p) basis set functions [30-31]. The electronic spectra of all molecules were calculated using the time-dependent density functional theory at the ωB97XD/cc-pVTZ level, as suggested by Harvey and co-workers, in a recent study of BODIPY derivatives [32]. Solvent effects on the electronic spectra calculations were treated using the linear response theory coupled with polarizable continuum model (LR-PCM)

[33], considering acetonitrile (MeCN) as solvent. All calculations were carried out using the C.01 version of Gaussian 09 program [34]. Reactive indexes were computed according to conceptual density functional theory formalism at the B3LYP-D2/cc-pVTZ level using the 3.7 version of Multiwfn program [35].

3. RESULTS AND DISCUSSION

In this section, we examine and compare the electrochemical and spectroelectrochemical behaviour of compounds **1**-**3,** and then undertake a computational study of the individual molecules, aiming to rationalize the electrochemical reaction mechanisms for the three compounds.

3.1 Electrochemical investigation

3.1.1 Reduction studies in DMF and MeCN by Cyclic Voltammetry (CV):

The electrochemical behaviour of 8-phenyl substituted BODIPY **1** and its nitrosyl derivatives **2** and **3** (Fig. 1) were investigated, using cyclic voltammetry (CV) (Fig. 2), in degassed DMF (Fig. 2) or MeCN + n-Bu_4NPF_6 solution (Fig. 3), at several scan rates, *vs*. Ag|AgCl|Cl^- (sat) [27].

In DMF, the CVs of compound **1** (Fig. 2A-C) in the range 0.5 V to –2.3 V, display, as expected, two reduction waves. The first is a chemically reversible wave and corresponds to a one-electron, quasi-reversible (EpIc_1 = -0.673 V and EpIa_1 = -0.588 V, ΔEp = 85 mV, dEp/dlgυ = -14.2 mV/decade), diffusion-controlled heterogeneous electron transfer process [36-37], yielding the corresponding radical-anion, with the electron added to the BODIPY core; the second is an irreversible process, (EpIIc_1 = -1.674 V, dEp/dlgυ = -70.4 mV/decade) (Figs. 2A and 2B) [37]. Assuming the molar volume of boron is that for carbon; that for fluorine is the same as for chlorine, and that the central 6-ring of the BODIPY core has the same molar volume as benzene, the Wilke-Chang approximation [38] may be used to estimate the diffusion coefficient (D) of **1** in DMF to be 1.5 x 10^{-5} cm^2 s^{-1}. This is in approximate agreement with that inferred from a Randles-Sevcík plot (not shown) of the peak current for the first

reduction wave (i_p) against the square-root of the voltage sweep rate, 2.8 ± 0.5 x 10^{-5} cm^2 s^{-1}, assuming electrochemical reversibility using equation (1),

$$i_p = 0.4463FSc_0\sqrt{\frac{DF\upsilon}{RT}} \quad (1)$$

in which F is the Faraday constant (96485.3 C mol^{-1}), S is the electrode area, R is the molar gas constant (8.3145 J mol^{-1} K^{-1}), *T* is the absolute temperature, c_0 is the concentration of **1** in the solution, and υ is the scan rate.

The large separation between peaks Ic and IIc (almost ~1.0 V) is well-known in the literature, and stems primarily from the orbital contributions, as estimated through computational analysis [13-17] (Fig. 2A-C). The irreversibility of the second wave is also well-recognised in the literature; as this compound has a plethora of unsubstituted positions, the electrogenerated dianion can undergo dimerization or other reactions, as is the present case, in terms of the second wave [15, 37]. This chemical reaction gives rise to a new anodic wave (IIa) around 0.0 V on the return sweep [37].

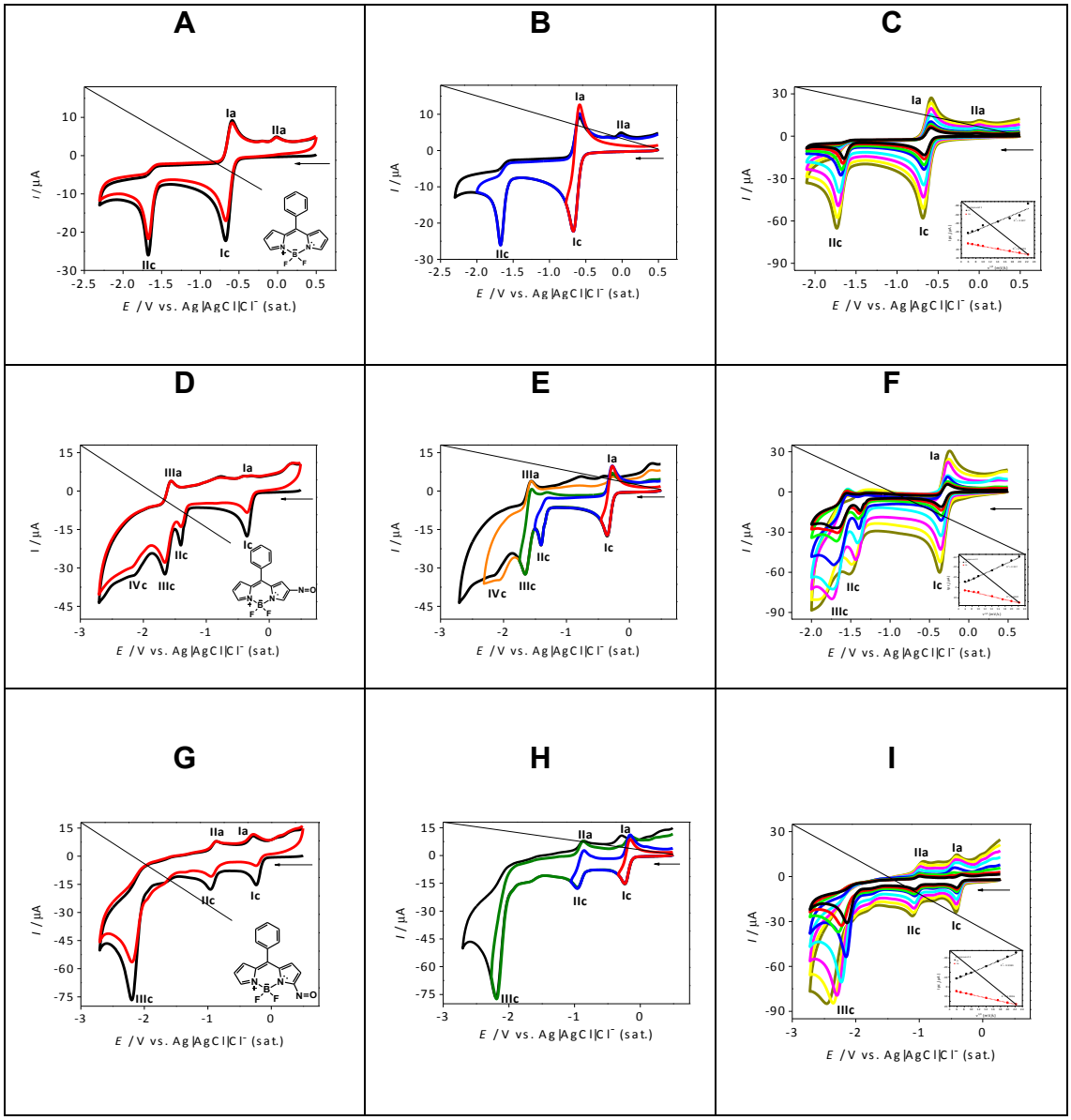

Figure 2. Cyclic voltammetry (CVs) of compounds **1** (A), **2**(D) and **3**(G) (1 x 10^{-3} mol L^{-1}) in DMF + $TBAPF_6$ (0.1 mol L^{-1}), *vs.* Ag|AgCl|Cl^- (sat.), GCE, υ = 100 mV s^{-1}. Successive CVs; black line – scan 1 and red line – scan 2. Several inversion potentials in the CV of compound **1**(B), **2**(E) and **3**(H). Scan rate effects in waves Ic and IIc for the compound **1** (C), **2** (F) and **3** (I) –dark yellow line: υ = 500 mV s^{-1}; yellow line: υ = 400 mV s^{-1}; magenta line: υ = 300 mV s^{-1}; cyan line: υ = 200 mV s^{-1}; blue line: υ = 100 mV s^{-1}; green line: υ = 75 mV s^{-1}; red line: υ = 50 mV s^{-1}; black line: υ = 35 mV s^{-1}. The arrow indicates the initial scan direction.

The addition of the electron-withdrawing nitrosyl group, in compounds **2** (in position β) and **3** (in position α), leads to different voltammetric profiles (cathodic direction**,** 0.5 V up to –2.7 V) (Fig. 2D-I). Compared with compound **1**, both compounds **2** and **3** are easier to reduce, with the first peak being 322 mV and 438 mV more positive than in compound **1**, respectively**.**

The CV profile of **2** is represented by four waves (Ic – IVc), with the first wave being slightly electrochemically *quasi*-reversible in nature (*E*pIc = -0.351 V; d*E*p/dlgυ= -9.6 mV/decade), and the second one being electrochemically irreversible, with a smaller current (*E*pIIc= -1.406 V; d*E*p/dlgυ = -50.3 mV/ decade). These first two waves are similar to those in compound **1**, and the peak current for the first reduction was found to be directly proportional to the square-root of the scan rate, as expected for diffusion-controlled behaviour, with a diffusion coefficient for compound **2** being determined as 1.5×10^{-5} cm^2 s^{-1}, which is commensurate with that estimated from the Wilke-Chang expression [38]. However, two additional waves are observable: whilst the third wave (*E*pIIIc = -1.653 V) appears to be chemically stable and reversible (there is a reverse peak), the fourth wave (*E*pIVc = -2.066 V) is broad and does not give a reverse peak.

In contrast, compound **3**, where the nitrosyl moiety is in the α-position, exhibits a more diverse profile, in comparison to compounds **1** and **2**, presenting three main waves (Ic, IIc and IIIc), with some shoulders (not assigned) (Fig. 2G-I) (Table 1). The two first waves are monoelectronic and display stable, electrochemically *quasi*-reversible electron transfers (*E*pIc = -0.238 V with d*E*p/dlgυ = -10.9 mV/decade and *E*pIIc = -0.957 V with d*E*p/dlgυ = -6.2 mV/ decade). These two waves are of equal height, and both have a similar dependence of peak current on square root of the scan rate, indicative of diffusion-controlled voltammetry. However, rather surprisingly, the size of the diffusion coefficient (6.1×10^{-6} cm^2 s^{-1}) is about one-half as large as both that of compound **2** (the positional isomer to **3**) and that estimated by the Wilke-Chang expression [38]. As with compound **2**, there is an additional wave at more negative potentials, but this is a single, third wave (*E*pIIIc = -2.201 V), and occurs with a much larger current than the first two waves. This third wave corresponds to a chemically irreversible process, that is of a diffusion-controlled

nature (peak current is directly proportional to the square-root of the voltage sweep rate).

Table 1 reports the main CV features for the contrasting behavior of all three compounds, quantitatively.

Table 1. Major electrochemical parameters (V) in CV (υ = 100 mV s^{-1}) of compounds **1**, **2** and **3** (c = 1 x 10^{-3} mol L^{-1}), in DMF + $TBAPF_6$, 0.1 mol L^{-1} and MeCN + $TBAPF_6$, 0.1 mol L^{-1}, *vs.* Ag|AgCl|Cl^- (sat.)

Solvent	Comp.	Reduction							Oxidation	
		*E*pIc	*E*pIa	Δ*E*p *mV*	*E*pIIc	*E*pIIa	Δ*E*p *mV*	*E*pIIIc	*E*pIIIa	*E*pIVa	*E*pVa
DMF	**1**	- 0.673	- 0.588	85	-1.674	-		-	-	*	*
	2	-0.351	-0.271	80	-1.406	-		-1.653	-1.559	*	*
	3	-0.238	-0.284	46	-0.957	-0.877	80	-2.201		*	*
MeCN	**1**	-0.745	-0.657	88	-1.710	-		-	-	+1.611	+1.920
	2	-0.408	-0.334	74	-1.360	-		- 1.604	-	+2.006	-
	3	-0.281	-0.210	71	-0.955	-0.876	79	-2.542	-1.565	+1.967	-

* not analyzed

In order to attempt to rationalize the differences observed in the voltammetry between **1**, **2** and **3**, CVs were also obtained in degassed MeCN + n-Bu_4NPF_6 solution, at several scan rates, *vs.* Ag|AgCl|Cl^- (sat.).

The reduction profiles of compounds **1-3** are very similar to the ones obtained in DMF, and are compared in Figure 3, with data additionally presented in Figures S2-S7 and Tables S1 and S2 in the Supplementary Information. Both anodic and cathodic peak currents vary approximately proportionally with the square-root of the scan rate over the range of 35 up to 1000 mV s^{-1}, which suggests that the process is predominantly diffusion controlled (Fig. 3D-F). Whilst the most negative potentials applied in the voltammograms suffer from interference of the solvent, there is a hint of a follow-on reduction for compound **1**, which may be similar to the wave corresponding to IIIc in **2** (with IVc) and **3**; this wave is due to complicated

multiple-electron waves with homogeneous reactions, and given the trace re-crossings (IIIc) at *ca.* -2.2 V, we suggest this corresponds to an ECE-type behaviour, since we were not able to find evidence of surface fouling during voltammetric cycling.

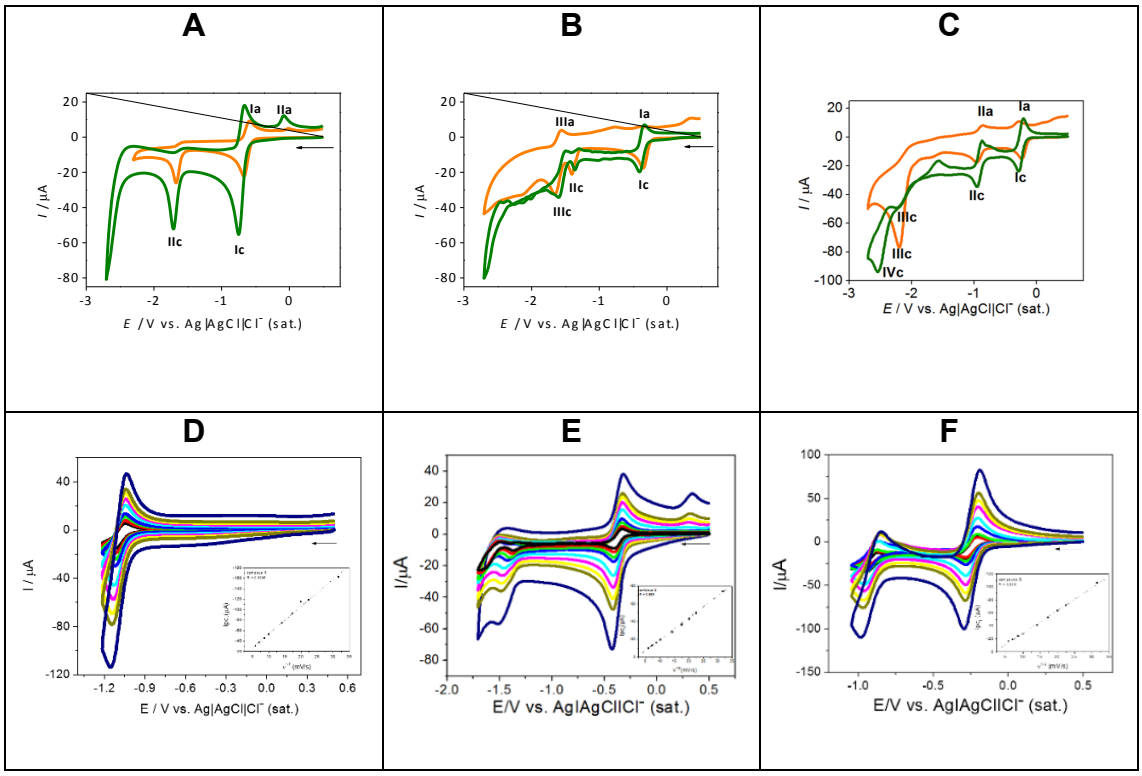

Figure 3. Comparison of CVs profiles, in MeCN and DMF of compounds **1** (A), **2** (B) and **3** (C) in DMF + $TBAPF_6$ (0.1 mol L^{-1}) (orange line) and in MeCN + $TBAPF_6$ (0.1 mol L^{-1}) (green line), *vs.* Ag|AgCl|Cl^- (sat.), GCE, υ = 100 mV s^{-1}. Cyclic voltammetry (CVs) of compounds **1** (D), **2** (E) and **3** (F) at different scan rates of 35, 40, 75, 100, 200, 300, 400, 500 and 1000 mV s^{-1} in MeCN + $TBAPF_6$ (0.1 mol L^{-1}).

It is particularly noticeable that for **1**, the peak currents in MeCN are approximately twice as large as those in DMF. This is exactly in line with expectation; the greater viscosity of DMF *c.f.* MeCN (0.794 cP *vs.* 0.369 at 298 K [39]) causes the estimated diffusion coefficient to be larger in MeCN (3.2 x 10^{-5} cm^2 s^{-1} [38]). Surprisingly, however, such a current doubling is not observed for **2** or **3**, indicating that additional phenomena occur. In fact, this in itself indicates that the hetero-aromatic nitroso moiety in compounds **2** and **3**

behave in line with aromatic *C*-nitroso species (Ar-N=O) through forming both *cis*- and *trans*-azodioxy dimers in solution (Ar-$N^+(O^-)$=$N^+(O^-)$-Ar) [24-26] (Figure 4).

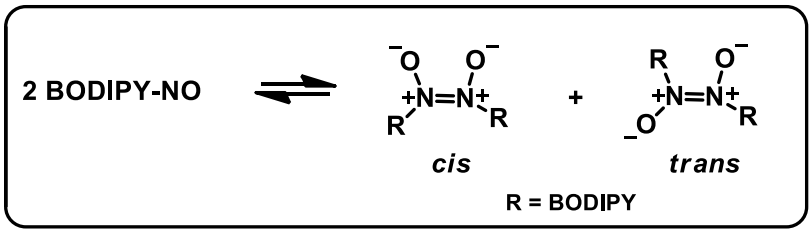

Figure 4. Putative scheme for the dimerization of nitrosyl derivatives, forming the *cis* and *trans* azodioxy dimers (adapted from [25]).

The formation of dimers has consequences for the electrochemical behaviour: following Simonet [26], we suggest that for **3**, the first two waves correspond to the reduction of the free monomer (M) and then the dimer (D), equations (2)-(6):

$$2M \rightleftharpoons D \quad (2)$$

$$M + e^- \rightleftharpoons M^{\bullet -} \quad (3)$$

$$D + e^- \rightleftharpoons D^{\bullet -} \quad (4)$$

$$D^{\bullet -} \rightleftharpoons M + M^{\bullet -} \quad (5)$$

$$Overall\,(3-5):\ D + 2e^- \longrightarrow 2M^{\bullet -} \quad (6)$$

Assuming the dimerization equilibrium (equation (2)) is slow on the voltammetric timescale, so that it is not significantly perturbed by the first electrode reaction (equation (3)), we can estimate the equilibrium concentration of both the free monomer (c_0-x) from the peak reduction current Ic, using the diffusion coefficient of **1** and the Randles-Sevcík equation (equation (1)). This enables the determination of the dimer concentration, through a mass balance, and

thence the equilibrium constant (*K*) for the dimerization process in equation (2), since this is given by equation (7):

$$K = \frac{x}{2(c_0 - x)^2} \qquad (7)$$

where x is the concentration of nitrosyl-BODIPY molecules that dimerise. We find that $K = 1.1 \pm 0.3\ M^{-1}$ for **3** in DMF and *ca.* $1.8\ M^{-1}$ in MeCN. This slight solvent effect is not unknown for *C*-nitroso aromatics [25]. Nevertheless, in both solvents, the dimer is estimated to have a *ca.* 10% smaller diffusion coefficient than the free monomers, based on the Wilke-Chang expression [38], so that in DMF, the approximately equal peak current for the first two waves results from the approximate 50/50 mixture of free monomers and dimer. In contrast, the slightly greater amount of dimer to monomer ratio in MeCN causes the second reduction wave (equation (4)) to be slightly larger than would be anticipated were the equilibrium constant to be independent of the nature of bathing medium.

In turning to compound **2**, we rationalize peak Ic in both DMF and MeCN as being due to the heterogenous reduction of the free monomer, equation (2); peak IIc as being the second electron heterogeneous reduction of the free monomer, given the similarity with **1**; and peak IIIc as being the mono-electronic heterogeneous reduction of the dimer, equation (3). Hence, analyzing the peak current of Ic for **2** in the same way as for **3**, we observe values of $K = 0.2 \pm 0.1\ M^{-1}$ in DMF and *ca.* $2.3\ M^{-1}$ in MeCN. This suggests that both neutral nitrosyl derivatives are more dimerised in MeCN than DMF, causing the dramatic apparent decrease in the peak currents compared with **1** on changing the solvent.

The extent of dimerization of **2** is only slightly greater than **3** in MeCN, but in DMF, that for **3** is an order of magnitude larger than for **2**. Nevertheless, it is surprising that the solvent effects for **2** are so much more marked than for its positional isomer **3**. Since DMF and MeCN are isodielectric [39,40], the extent of dimerization controlled by dipole-dipole interactions [25] is likely to be similar in both solvents. However, DMF has a greater value of the Gutman donor number than MeCN [40]. This number recognizes the ability of a solvent to promote the ionization of compounds to form ion pairs, so we would expect

greater stabilization of the dimer in DMF than in MeCN. The fact that the converse is seen, suggests that the solvent plays a nucleophilic role: Gal and Maria noted that the enthalpy of complex formation with BF_3 is greater (-110 kJ mol^{-1}) for DMF than for MeCN (-60 kJ mol^{-1}) [41]. We thus rationalise the greater dimerization in MeCN through the competition between the molecular dimerisation of the neutral nitrosyl moiety illustrated in Figure 4, with solvent co-ordination to the $-BF_2$ moiety of the boron-substituted ring. Since DMF is more basic, provided there are no steric effects, solvent co-ordination to the central ring will favour monomers over the dimer. In contrast, solvent co-ordination by MeCN is weaker, so that in this solvent, dimerisation is likely to be more thermodynamically favoured. This explains why compound **2** exhibits marked solvent-dependent behaviour, whilst in the positional isomer, compound **3**, steric effects reduce the interaction of the solvent with the central ring, and so the solvent effect is lower. Compound **1**, like compound **2**, has no steric constraints, and no competing dimer, so that it exists only as a monomer.

In the above, we have not been able to discern whether the dimers for **2** and **3** exists in *cis* or *trans* form; it is clear, however, that the extent of dimerization will be more affected by steric constraints for the *cis*-isomer, than for the *trans* one.

We next investigate the oxidative voltammetry of the compounds.

3.1.2 Oxidation studies in MeCN by Cyclic Voltammetry (CV)

In the oxidation region, obtained in MeCN + $TBAPF_6$, the CV profiles, with peaks at very positive potentials are related to irreversible electron transfers for compounds **2** (*E*pIVa = 2.006 V) and **3** (*E*pIVa = 1.967 V), differently from the behaviour of compound **1**, which is represented by two peaks (*E*pIIIa = 1.610 V and *E*pIV = 1.920 V) (Fig. 5). The nitrosyl substitution at positions β and α of compounds **2** and **3** strongly affects the oxidation, with anodic shifts of 0.396 V and 0.357 V, respectively. Given that the concentrations of the compounds (c = 1 x 10^{-3} mol L^{-1}) and the scan rates (υ = 100 mV s^{-1}) are the same (c = 1 x 10^{-3} mol L^{-1}) in both Figures 3 and 5, and

since, for **1**, peak Ic corresponds to the transfer of a single electron per mole, we suggest that wave IVa for **1**, corresponds to a multistep electron transfer process, with the electron first being removed from the BODIPY core [12-23]. The similarity between **2** and **3**, but the difference with **1**, likely indicates the involvement of the unstable cation radical of the aromatic nitroso moiety [42]. For **2** and **3,** the signal occurs very close to the limit of the solvent window, so that it is not possible to rationalize whether the observed peak derives from the free monomer or the dimer. However, the increased current compared with peak Ic for **2** and **3** indicates the possible occurrence of an ECE or DISP-type mechanism.

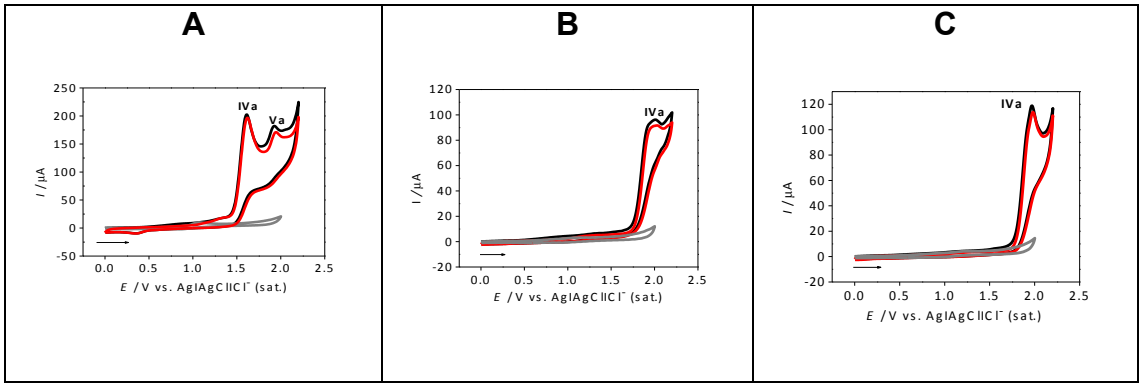

Figure 5. CVs profiles of compounds **1** (A), **2** (B) and **3** (C). Black line – scan 1 and red line – scan 2. MeCN + $TBAPF_6$ (0.1 mol L^{-1}), *vs.* Ag|AgCl|Cl^- (sat.), GCE, υ = 100 mV s^{-1}.

Table 1 lists the main electrochemical data, including for oxidation, obtained under different conditions.

In order to fingerprint species and rationalise the mechanisms suggested by the voltammetric measurements, we next consider the *in situ* spectroelectrochemical probing of the reaction intermediates.

3.1.3 *In situ* UV-vis spectroelectrochemistry in aprotic media

UV-vis absorption spectra for all BODIPY compounds, recorded in dilute solutions in either DMF + $TBAPF_6$ 0.1 mol L^{-1}, are illustrated in Figure 6, with peak maxima and their movements presented in Table 2. Although different solvents were used in the literature, and given that the absorption spectra are

dependent on solvent polarity, our spectroelectrochemical investigations of the three compounds were undertaken in DMF and MeCN electrolyte solutions for reduction, and in MeCN, for oxidation, owing to the impurities present in our DMF electrolytes apparent on oxidation (Figure S1 of the Supplementary Information). It is clear from Figure 6 that the absorption spectra are similar to other, structurally related, BODIPY [8 and included references], with an intense absorption band around 500 nm and a less pronounced shoulder at shorter wavelengths [8]. In DMF, compounds **1** and **2** behave similarly, as may be expected from the voltammetric investigation, with **3** affording different features.

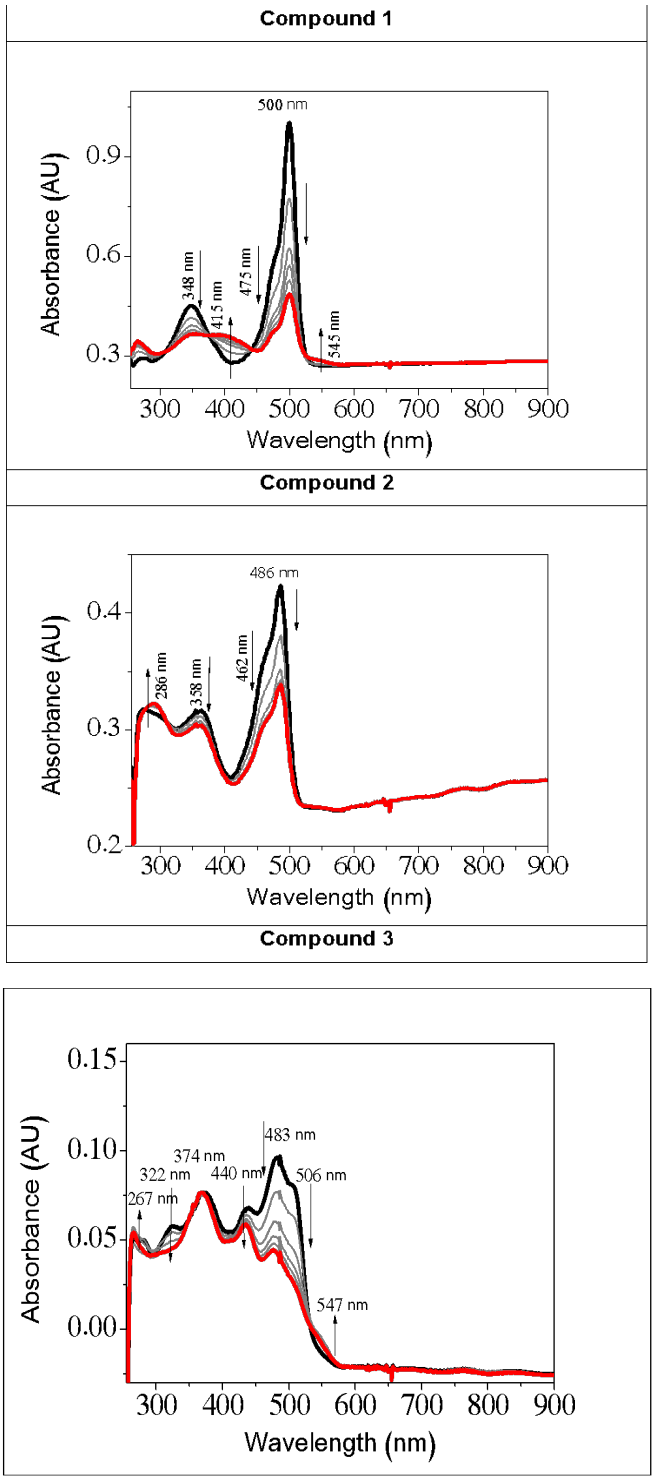

Figure 6. (Solid black line) UV-VIS initial spectra in DMF + $TBAPF_6$ 0.1 mol L^{-1} (optical path 1 cm, of compounds **1, 2** and **3** (*c* = 2.5 mmol L^{-1}). Spectroelectrochemical experiment, on Pt grid working electrode. (Grey and red solid lines) UV-VIS spectra during the reduction (0 to -1.5 V), with the red line representing the final scan.

The absorption spectrum of compound **1** (Figure 6A) is analogous to that in cyclohexane, exhibiting two main absorption bands: a strong intensity peak in the visible wavelength region, related to the S_0-S_1 transition, with a maximum at 500 nm (Table 2) with a shoulder at 475 nm, and a much less pronounced band towards higher energy (348 nm). The latter is attributed to the 0-1 vibrational band of the same transition. The wavelengths of these absorption maxima λ_{abs} (max) (Table 2) are very similar to those of other typical BODIPY derivatives [8], and these also depend on the solvent, as common for this class of dyes [43-44]. Indeed, in MeCN, there is a small (*ca.* 3 nm) hypsochromic shift of the peak maxima (see Figure S8 of the Supplementary Information).

Compound **2** exhibits similar features to **1** – there is a main wave, with the wavelength of maximum absorption (λ_{abs} = 486 nm) being slightly hypsochromically shifted compared with **1**, with a higher energy shoulder to this wave (462 nm). This main wave is further shifted to 483 nm for **3**, which affords a remarkably distinct spectrum (*vide infra*). In both **2** and **3**, this main wave is attributed to n - π* transitions [43-45]. The hypsochromic shift that is observed is similar to that described in the literature for 6-nitro and 5-nitro-BODIPYs [46]. The plausible explanation in this case is due to its electron-withdrawing character, which removes part of the electronic density delocalized through the BODIPY core [46].

Other less intense bands exist between 267-374 nm in the spectra of **1**-**3**, however these are more intense for **1** and **2** compared with **3**. The blue-shifts of the absorption bands in this region (267-374 nm), may also be related to the free rotation of the 8-phenyl ring due to the lack of substituents at the adjacent 1 and 7 positions of the BODIPY core and at the *ortho* positions of the 8-phenyl moiety [44-45].

The spectrum of compound **3** is more complex than **2**, with the main intensity band occurring at 483 nm, with a bathochromic shoulder at 506 nm, so that this band appears to be split into at least two transitions. Three further peaks are also observed at higher energy, corresponding to wavelengths of

440, 374 and 322 nm, with an additional UV peak at 267 nm. As for **2**, some higher energy bands are related to the presence of the nitrosyl group, as shown for nitrosobenzene derivatives [47-49]. Similar behaviour is seen for **3** in MeCN solution (see Figure S9 in the Supplementary Information).

Compared with **1**, the peak intensities (and areas) of the main absorption band are significantly smaller for **2** and **3**. We suggest that this significant deviation in the absorption spectra for **2** and **3** compared with **1** corresponds to the dimerization process indicated by the voltammetric data described in section 3.1.1 above. Indeed, it is often assumed that the azodioxy dimer (Figure 5) does not absorb at the wavelength corresponding to the monomeric main peak [48]. Thus, taken together, this suggests that the extent of the monomer/azodioxy dimer equilibrium for **2** and **3** in DMF is greatest for **3**, but is still important for **2**. We are not able to discern the structure of the azodioxy dimer from UV-visible spectroscopy [25].

Table 2. UV-visible data and alterations due to applied potentials, by spectroelectrochemistry, held in DMF + $TBAPF_6$ 0.1 mol L^{-1}.

			APPLYING FOR 120 s (V) (nm)					
COMPOUND	**INITIAL PROFILE (nm)**	**DURING THE REDUCTION (nm)**	**- 0.25**	**- 0.35**	**- 1.00**	**- 1.40**	**- 1.60**	**- 1.70**
1	**275; 348; 475; 500**	**348↓; 415↑ ; 475↓; 500↓; 545↑**			**266↑; 348; 415 475↓; 500 545↑**		**266↑; 348↓; 415 475↓; 500↓ 545↑**	
2	**266; 358; 462; 486**	**286↑; 358↓; 462 ↓; 486↓**		**268; 364↓; 462↓; 486↓**		**294; 364↓; 462↓; 486↓**		**294; 364↓; 462↓; 485**

3	**283; 322; 374; 440; 483; 506**	**267↑; 322↓; 374; 440↓; 483↓; 506↓ 547↑**	**322↓ 370; 435; 483↓; 506↓; 547↑ 801↑**		**267; 370; 432; 473↓**			

During the course of reductive electrolysis of all three compounds, the strong absorption band decreases in intensity, as expected for conversion of the neutral compounds to their reduced forms. This creates a new absorbing species, as evidenced by the emergence of a peak at 415 nm (for **1**) and an increase in the signals at 286 and 267 nm for **2** and **3**, respectively (Fig. 6, Table 2) [46].

Figure 7 illustrates the variation of the UV-visible absorption spectra as the working electrode potential is swept towards more negative potentials. Reduction of **1** at two different potentials (-1.0 V and -1.6 V), in DMF + $TBAPF_6$, causes a decrease in the intensity of the absorption bands at 500 and 348 nm and the appearance of a very-low intensity band at 544 nm and one at 400 nm. This behaviour is similar to the that displayed by the same compound in CH_2Cl_2 [12] and also in MeCN [37] (see also Figure S8 of the Supporting Information), and is related to the formation of the corresponding anion radical, as demonstrated in the literature using electrochemistry with *in situ* monitoring using electron paramagnetic resonance [12]. An isobestic point is observabale at 389 nm. Small bathochromic shifts (around 15 nm in the higher energy region and around 30-80 nm at the visible region) were reported for the possible dimers (α,α- and β,β-), in different solvents, such as THF and MeCN [8,17,44-45].

The spectroelectrochemical profile of compound **2** is surprising: despite the presence of the nitrosyl group, the resulting electronic spectra, upon reduction, are similar to the one from compound **1** (Fig. 7), albeit with a main wave of reduced intensity. We propose that this is in agreement with the notion that azodioxy formation of the neutral species exists for compound **2** in DMF

electrolytes; owing to the change in the extinction coefficient, we are unable to use these data quantitatively to corroborate the equilibrium constant estimated voltammetrically.

In contrast, compound **3** exhibits a markedly different spectroelectrochemical profile on reduction. Over the time-course of electrolysis, one band at the visible region with a maximum at 560 nm was observed, together with a decrease in the intensity of the strongly absorbing band (Fig. 7). Prior to the onset of the electrolysis, little, if any, absorption above 550 nm exists, which suggests that these two peaks indicate the presence of a new solution phase species, possibly the nitroso radical anion, as observed previously [47-48].

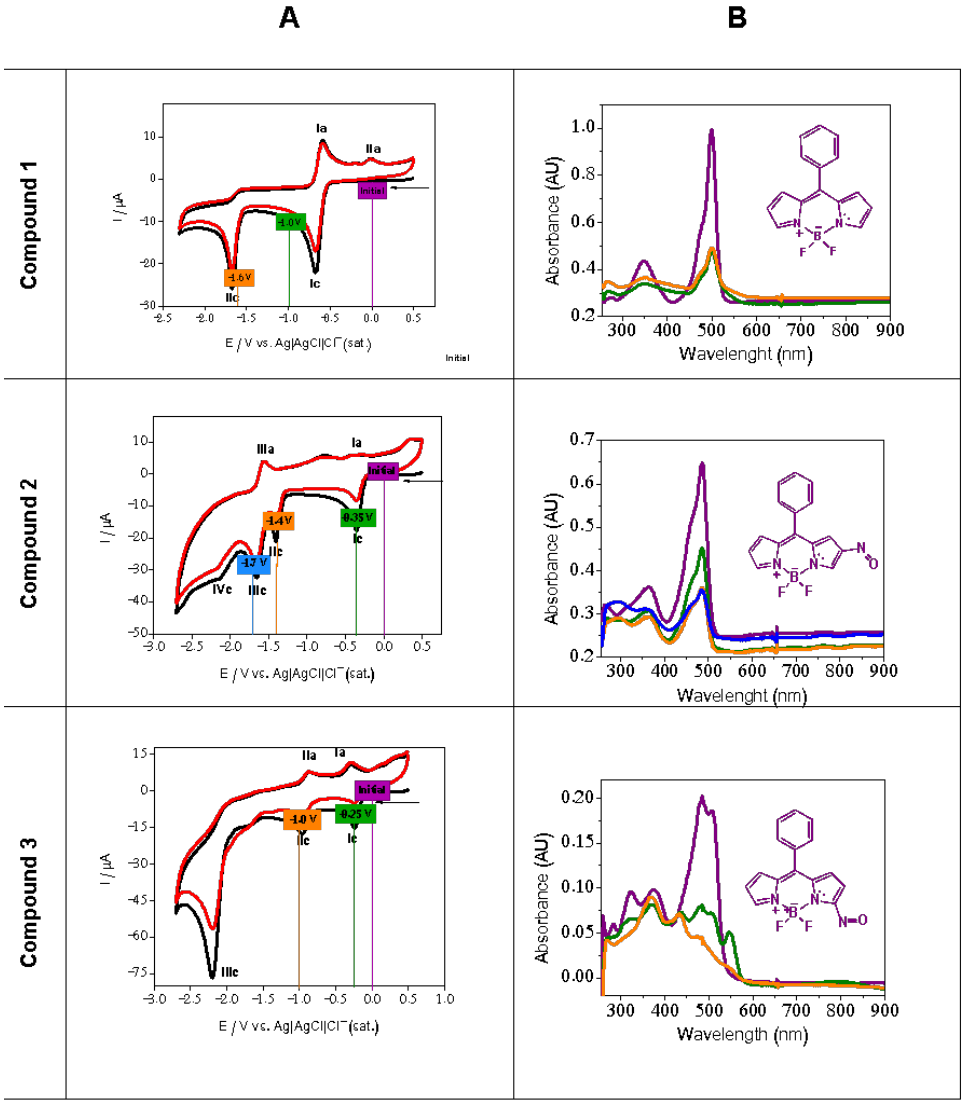

Figure 7. (**A**) Successive CVs (100 mV s^{-1}) of compounds **1**-**3** with values of applied potential in UV-vis spectroelectrochemistry (**B**) *In situ* UV-vis spectroelectrochemistry obtained in an optically transparent thin layer electrochemical cell, using Pt grid working electrode, during the constant potential reduction of 2.5 x 10^{-3} mol L^{-1} compounds **1**-**3** in DMF + $TBAPF_6$, 0.1 mol L^{-1} (purple line: the UV-vis spectra of oxidation state of compounds **1**-**3**; green line: the UV-vis spectra were obtained after applying for 120 s a reduction potential of - 1.0 V (**1**), - 0. 35 (**2**) and – 0.25 V (**3**); orange line: the UV-vis spectra were obtained after applying for 120 s, a reduction potential of –1.6 V (**1**), –1.4 V (**2**), –1.0 V (**3**); blue line: the UV-vis spectra were obtained after applying for 120 s a reduction potential of –1.7 V (**2**).

The spectroelectrochemical reduction of **3** in MeCN behaves similarly to DMF (Figures S9 and S10 of the Supplementary Information), except that in this solvent, the peak at 478 nm increases after the first reduction wave, and subsequently decreases after the second reduction. This indicates that the dimerization equilibrium (equation (2)) is dynamic, and slow kinetics serve as a good first approximation.

In terms of oxidation of compound **1**, upon maintaining the working electrode potential at +1.30 V for 120 s in MeCN, the absorption spectrum retained the profile of the neutral species, except with a decrease in the intensity, and the appearance of a red-shifted band, located at 534 nm, which corresponds to the oxidised product (Fig. 8) [50].

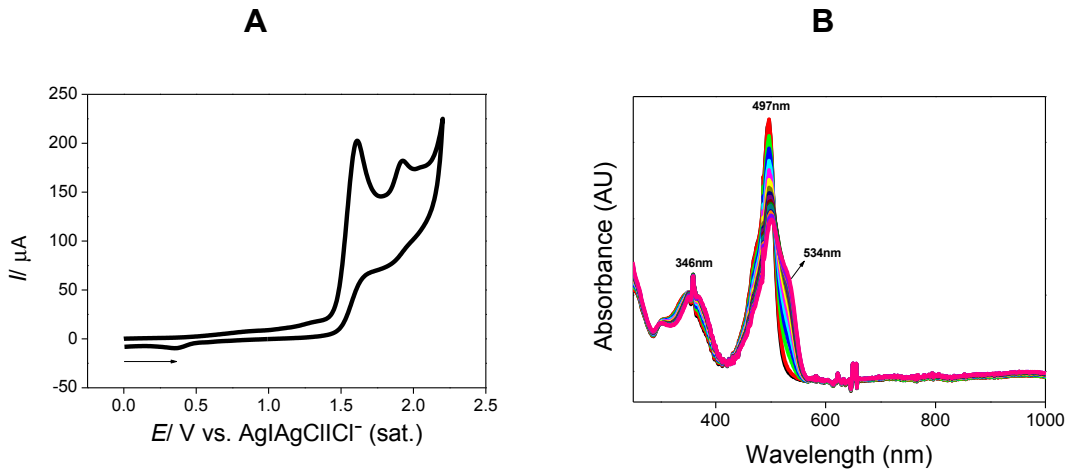

Figure 8. CV of compound **1**, in MeCN + $TBAPF_6$ (0.1 mol L^{-1}), GCE, υ = 100 mV s^{-1}. (**A**) CV of compound **1** (2.5 x 10^{-3} mol L^{-1}). MeCN + $TBAPF_6$ (0.1 mol L^{-1}), GCE, υ = 100 mV s^{-1}. (**B**)The UV-vis spectra were obtained after applying for 120 s, an oxidation potential of +1.30 V.

In order to rationalise the underpinning molecular factors giving rise to these experimental results, a computational study was undertaken. This is next described.

3.2 Computational Study

It is important to emphasize that this study was undertaken considering only the monomer species; this impacts on the first reduction waves, and it is well known that the monomer is the first to be reduced [26].

A Conceptual Density Functional Theory (CDFT) was used to unravel additional details regarding how the position (α or β) of the nitroso group in the pyrrole ring of 8-phenyl-BODIPY (**1**) would affect the electronic structure, and consequently, the electronic properties of nitrosyl BODIPY (compounds **2** and **3**).

Accordingly, plots of the condensed Fukui functions calculated for the 8-phenyl-BODIPY (**1**) and nitrosyl derivatives (**2** and **3**) are depicted in Figure 9.

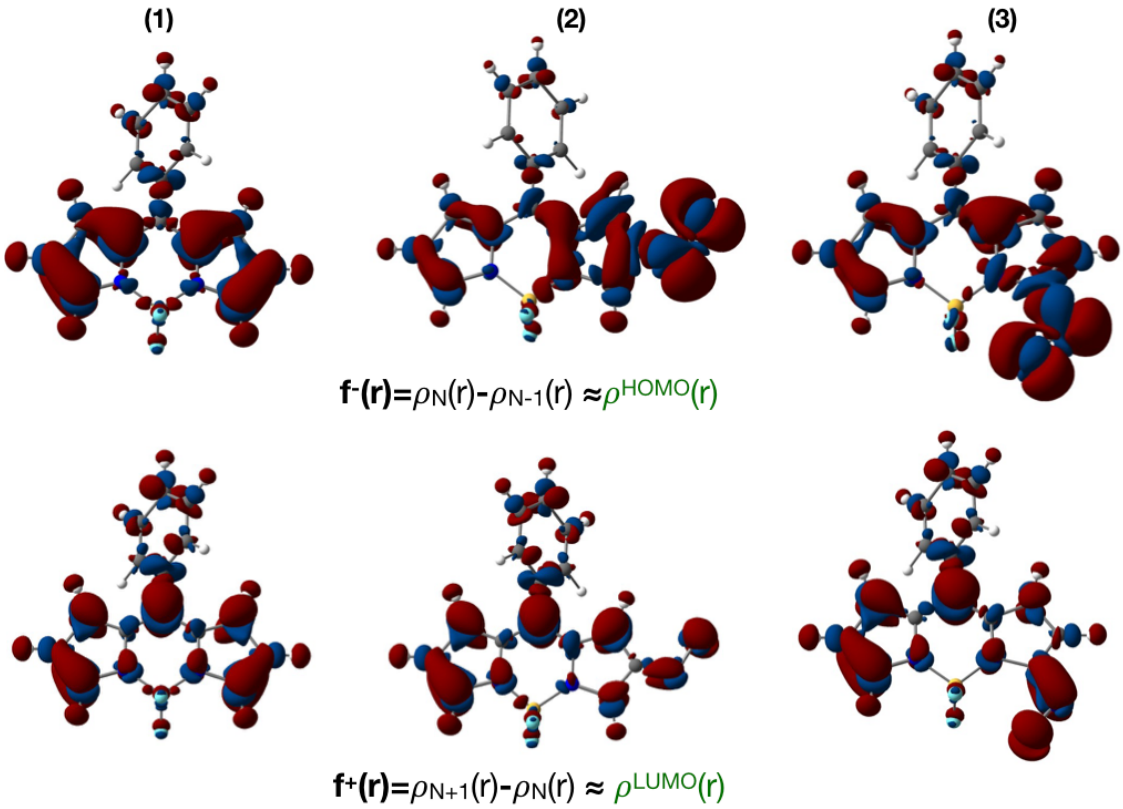

Figure 9. Condensed Fukui function calculated at the B3LYP-D2/cc-pVTZ level of theory for 8-phenyl-BODIPY (**1**) and its nitrosyl derivatives (**2** and **3**). Positive and negative values are in red and blue, respectively. N is the number of electrons of the respective molecules.

B3LYP-D2/cc-pVTZ calculations indicate that the presence of the nitrosyl group (compounds **2** and **3**) in the 8-phenyl-BODIPY (**1**) core change the density of the HOMO orbital (f^- function) considerably in comparison to the standard NO free-compound **1** (see Figure 1 or structures in Figure 9). As can be seen, in compounds **2** and **3**, the central part of the density of the HOMO orbital is distributed over the NO group. According to Fukui functions formalism, positive values of the f^- function characterize sites in a molecule more susceptible to suffer an electrophilic attack. Thus, analysing the variation of the plot density of the HOMO orbital in Figure 9, it is plausible to suggest that the addition of the NO group into the BODIPY core changes the main electrophilic reactive centers from the pyrrole rings toward NO.

Table 3 shows the vertical ionization potential and the electron affinity band of the 8-phenyl-BODIPY (**1**) and nitrosyl (**2**) and (**3**) derivatives.

Table 3. Calculated vertical Ionization Potential (VIP) and Vertical Electron Affinity (VEA) according the conceptual density functional theory at the B3LYP-D2/cc-pVTZ level. *E* is the total energy and N is the number of electrons of the respective molecules.

Comp.	E_N (a.u.)	E_{N-1} (a.u.)	E_{N+1} (a.u.)	VIP (eV)	VEA (eV)
1	-912.757386	-912.473076	-912.817771	7.73	1.64
2	-1042.093670	-1041.808401	-1042.177413	7.76	2.28
3	-1042.083601	-1041.80782	-1042.170733	7.50	2.37

According to Table 3, the insertion of NO into the pyrrole ring of BODIPY does not significantly alter the vertical ionization potential (VIP)l concerning 8-phenyl-BODIPY. On the contrary, the vertical electron affinity (VEA) analysis clearly shows the electronic differences between the three compounds investigated. As can be seen, about compound **1**, the NO group entrance into the BODIPY moiety promotes a considerable increase of the energy required to detach the electron from the singly negative charged molecular ion, which means that the NO addition to BODIPY core increases the vertical electron affinity, in line with experimental data. These computational results also suggest that the position of the nitroso group in the α position, facilitates the reduction process of BODIPY derivative compounds compared to 8-phenyl-BODIPY (**1**), as also observed experimentally.

Figure 10 depicts the UV/vis spectra of 8-phenyl-BODIPY (**1**) and nitroso derivatives, calculated at the ωB97XD/cc-pVTZ /PCM($\sum$=37.219) level..

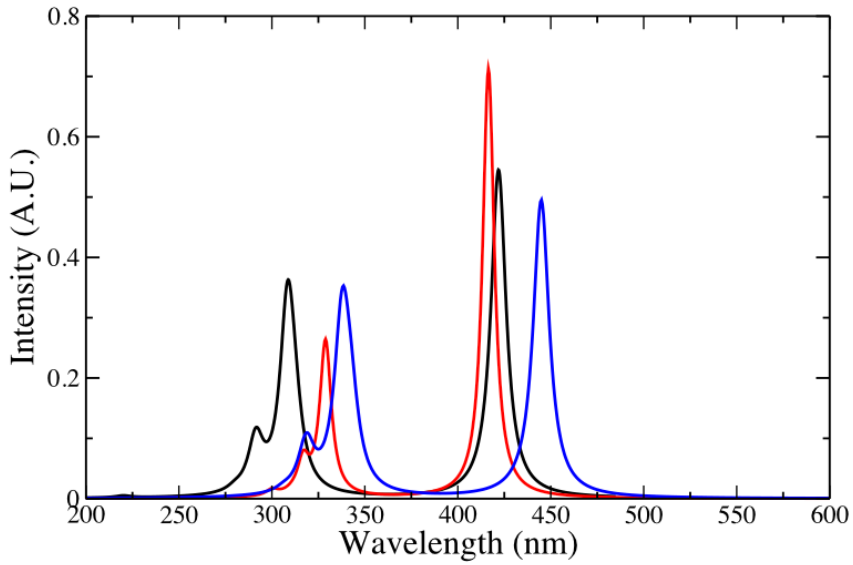

Figure 10: Calculated UV/vis spectra of compound **1** (black), **2** (red) and **3** (blue).

The spectroelectrochemical study of compound **1** reveals two initial bands at around 273 and 348 nm, which are in reasonable agreement with values of 290 and 303 nm calculated at ωB97XD/cc-pVTZ /PCM($\sum$=37.219) level.

Spectroelectrochemical results also revealed the appearance of an intense band at ~ 500 nm. Regarding this band, the theoretical results predicted a value of ~ 415 nm, which in this case shows a reasonable agreement, at least in a semi-quantitative mode. For all three systems, the theoretical results characterize the respective more intense bands relative to electronic transitions involving the HOMO-LUMO orbitals of each species, whose orbitals are shown in Figure 11.

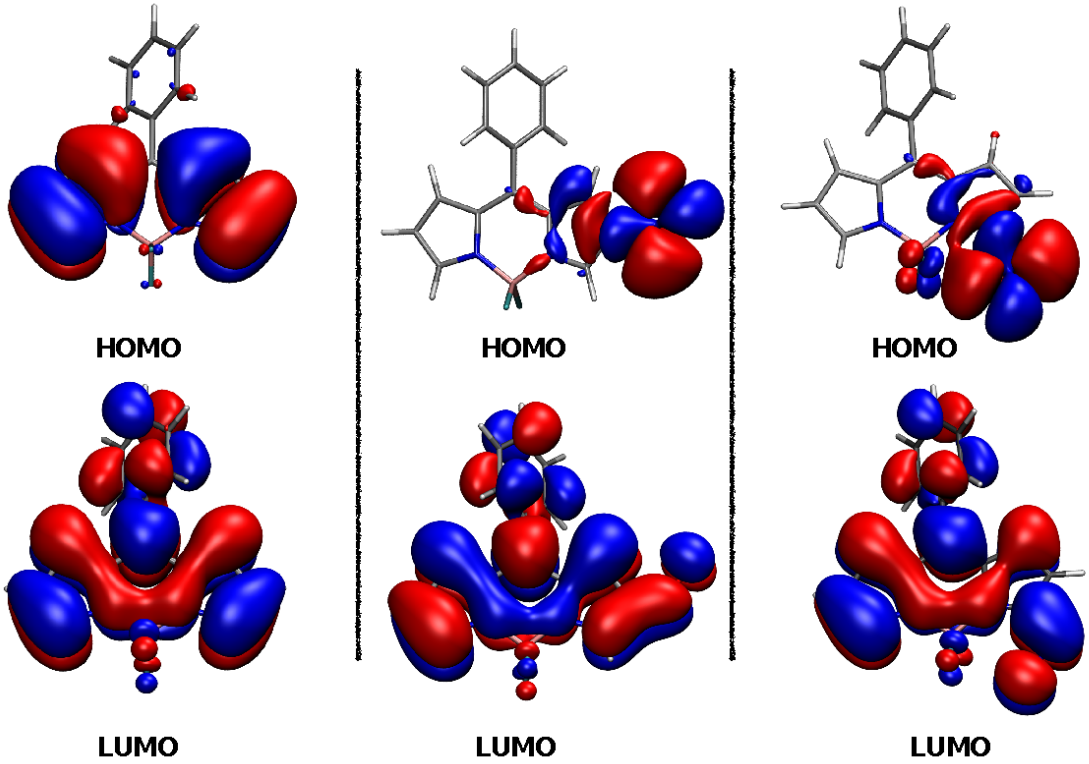

Figure 11. Kohn-Sham frontiers molecular orbitals of the 8-phenyl-BODIPY (**1**) and BODIPY nitroso derivatives (**2**) and (**3**).

The analysis of the Kohn-Sham frontiers molecular orbitals shown in Figure 11 indicates that the HOMO-LUMO electronic transition is essentially characterized by a charge transfer (CT) from NO group to the BODIPY moiety in compounds **2** and **3**. Table 4 shows the main components of HOMO orbital for the investigated nitrosyl-BODIPY compounds, analyzed according to the natural orbital method [33,35].

Table 4. Natural atomic orbital (NAO) analysis of the HOMO orbital of compounds **2** and **3**.

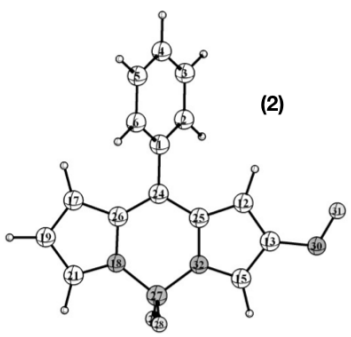

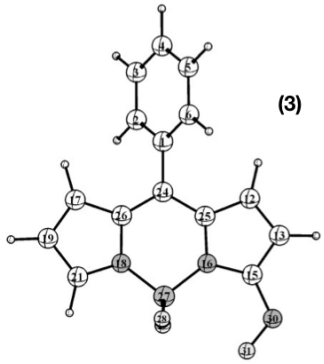

	HOMO - Compound 2		HOMO - Compound 3	
Atom	**Type**	**Composition (%)**	**Type**	**Composition (%)**
12 C	2px	1.266	-	-
13 C	2s	1.348	-	-
13 C	2py	3.656	-	-
15 C	-	-	2s	1.785
15 C	-	-	2px	3.581
16 N		-	2px	0.770
30 N	2s	7.885	2s	7.779
30 N	2px+py	27.844	2py	26.788
31 O	2px+2py	55.795	2px+2py	55.895

The data in Table 4 show clearly, as also indicated by Figure 11, that the HOMO orbital of compounds **2** and **3** is essentially composed (> 82 %) by p orbitals of the NO group. Concerning LUMO orbital, the natural atomic orbital analysis indicates that the main contributor (~90%) is the π orbitals from the BODIPY core.

Similar to observed concerning compound **1**, our computational results also do not accurately characterize the band's appearance at 506 nm observed experimentally, after reduction for compound **3**. Nevertheless, in line with the spectroelectrochemical findings, the computational results indicate that incorporating the NO group in the BODIPY molecule promotes a red-shift displacement concerning the more intense bands measured for the three investigated compounds. Besides that, the qualitative analysis of Kohn-Sham frontier molecular orbitals and the calculated electronic spectra suggest that the interaction between the nitroso group and fluorine atoms of BODIPY moiety can play an important role in the electronic properties of these systems. For example, comparing with compound **2** (curve in red), the NO---Fluorine interaction in **3** (curve in blue) promotes an offset around 30 nm toward the red region, which is in good agreement with the measured value of ~ 22 nm taking as reference the difference between the bands at 506 nm (in **3**) and 486 nm (in **2**).

We next consolidate the insights from the previous sections through developing plausible mechanisms to account for the electrochemical processes observed.

3.3 Mechanistic Rationalization

Putative schemes for the reduction and oxidation pathways, based on the combined results are presented in Figure 12. Compound **1** is thought to be reduced in two one-electron steps (Fig. 12A), with the second reduction being chemically irreversible. Both electrons are introduced into the BODIPY core.

Compound **3** (Figure 12C) exists as both free monomer and azodioxy dimer. In both DMF and MeCN, the monomer is reduced in a one-electron wave first, with the electron being accepted on the nitrosyl moiety. The dimer is then reduced in a one-electron wave, to afford the dimer anion-radical, which can break-up to yield the free monomer and the monomer anion radical. In MeCN, the anion radicals of the dimer and the monomer appear to be further reduced separately, with protonation events, presumably to the hydroxylamine.

These processes are not readily discernable in DMF, where a single broad voltammetric wave appears.

Compound **2** appears to follow a mechanism that is mixed between the two extremes of **1** and **3**: it dimerises, and it exhibits reduction through the BODIPY core, where two one-electron waves are observed for the monomer. The second of these waves is fast in chemical follow-on reaction, but it is at a potential that enables self-redox catalysis of the dimer to its anion radical, with follow-on reactions.

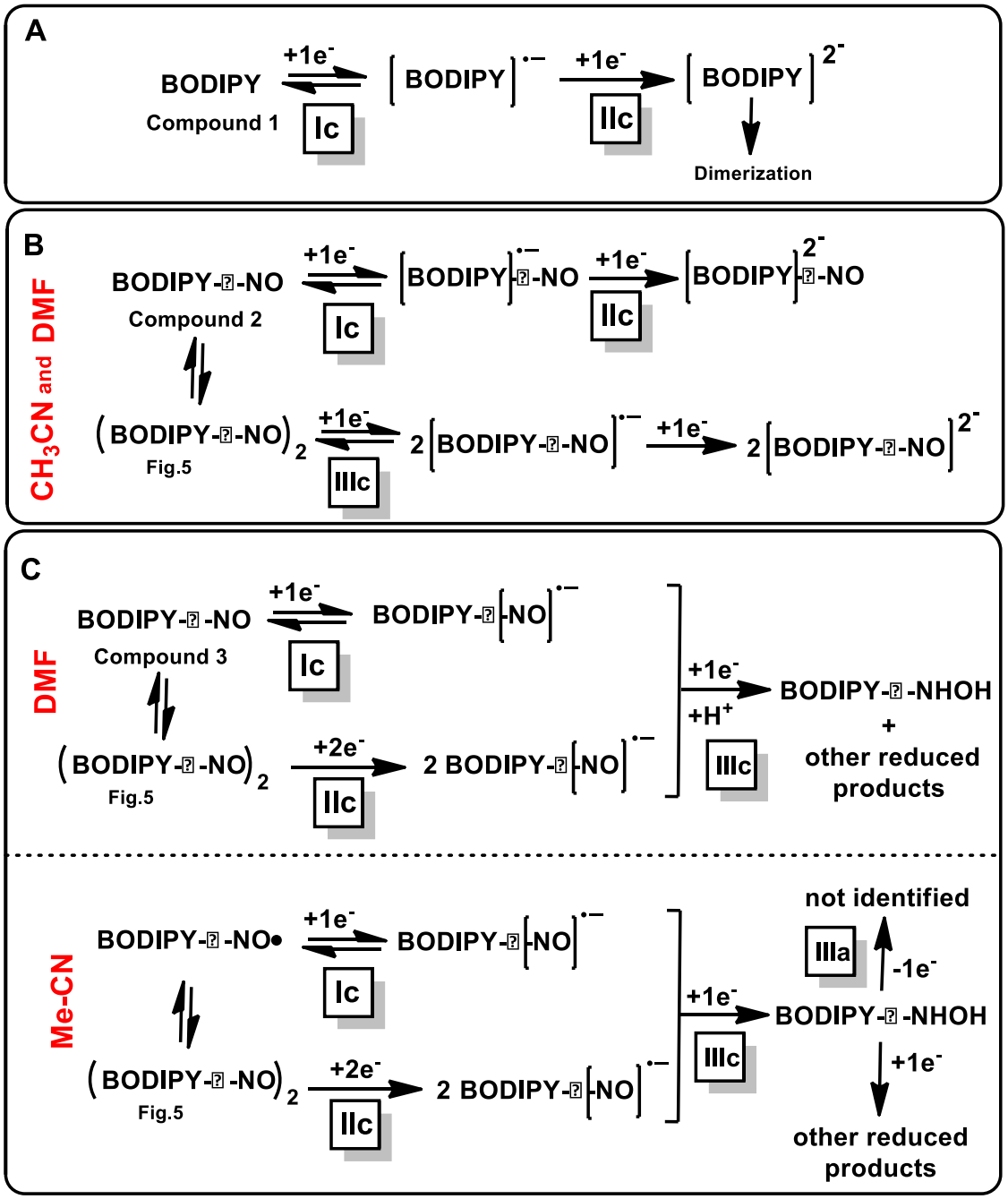

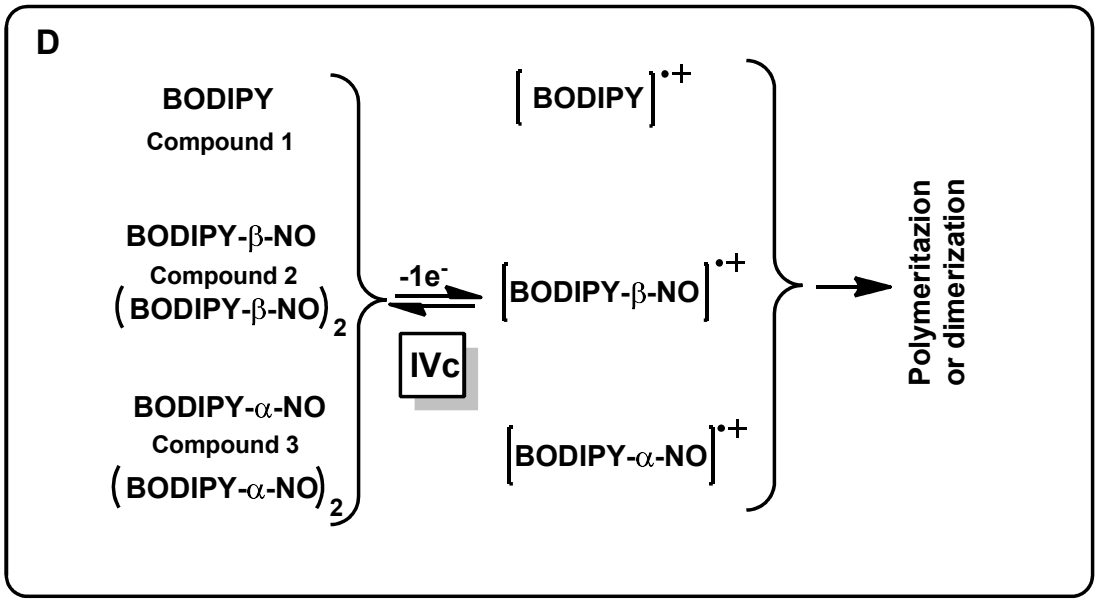

Figure 12. Putative schemes related to the reduction (A-C) and oxidation (D) of compounds **1**, **2** and **3**.

4. CONCLUSIONS

In this work, new nitrosyl BODIPY dyes [6] have been investigated by electrochemical and optical means. The studies have highlighted the influence of solvents and the essential role of the nature and position of the *C*-nitroso substituent.

The substitution at positions 5 (**3**) and 6 (**2**) with this previously unstudied electron-withdrawing group with non-bonding electrons, enables the tuning of the redox potentials. One of the most surprising features observed in this work is the extent to which the nature of the polar, aprotic solvent enables the discernment of the mixed mechanism for **2**, by changing the monomer-to-azodioxy dimer ratio.

Reversible dimerization, one of the most characteristic and puzzling properties of aromatic *C*-nitroso compounds and their heteroaromatic analogues, has remained mysterious for decades, and it is only recently that a fuller understanding of the whys and wherefores of this process has finally begun to emerge. Improved knowledge of the behaviour of these compounds is beginning to shed valuable light on the study of many other areas of chemistry.

At the same time, new ways to exploit the reversible dimerization of nitrosoarenes are being discovered [25].

According to results obtained *via* CDFT, the addition of the NO group to the BODIPY core changes the main electrophilic reactive centers from the pyrrole rings toward NO. In line with the experimental findings, the calculated vertical electron affinity of the three investigated compounds revealed that incorporating NO in BODIPY moiety facilitates the reduction process. The frontier molecular orbitals analysis showed that the more intense absorption bands in the BODIPY and BODIY-NO derivatives compounds are mainly characterized through a charge transfer mechanism (CT) from NO group to BODIPY core. The qualitative analysis of Kohn-Sham frontier molecular orbitals and the calculated electronic spectra pointed that the interaction between nitroso and fluorine atoms of BODIPY moiety can play an important role in the electronic properties of these systems, promoting a bathochromic offset.

These studies highlight that the reduction mechanisms for **1** and **3** are two dichotomic pathways of a continuous mechanistic spectrum, with **2** following a mixture of the two extremes.

Acknowledgments

The authors acknowledge the São Paulo Research Foundation (FAPESP – grant #2011/23342-9; FAPESP – grant #2014/18973-8; FAPESP – grant #2013/50677-7), the CNPq (Conselho Nacional de Desenvolvimento Científico e Tecnológico, APQ-CNPq ID: 421701/2018-8, CNPq 435704/2018-4), Instituto Nacional de Ciência e Tecnologia, INCTBIO (Process 465389/2014-7) and Fundação de Amparo à Pesquisa do Estado de Alagoas (FAPEAL). The authors also thank the LQTC (Laboratório de Química Teórica e Computacional, Universidade Federal de Pernambuco) for the computational resources used to perform part of the calculations.

REFERENCES

[1] L. D. Lavis, R. T. Raines, *ACS Chem. Biol.* **2008**, *3*, 142–155.

[2] A. Treibs, F.-H. Kreuzer, *Justus Liebigs Ann. Chem.* **1968**, *718*, 208–223.

[3] N. Menges, *Comput. Theor. Chem.* **2015**, *1068*, 117–122.

[4] A. Loudet, K. Burgess, *Chem. Rev.* **2007**, *107*, 4891–4932.

[5] G. Ulrich, R. Ziessel, A. Harriman, *Angew. Chemie Int. Ed.* **2008**, *47*, 1184–1201.

[6] S. Swavey, M. Coladipietro, A. Burbayea, J. A. Krause, *Eur. J. Org. Chem.* **2016**, *2016*, 4429–4435.

[7] S. M. Gil de Melo, L. C. D. de Rezende, R. Petrilli, R. F. Vianna Lopez, M. O. F. Goulart, F. da Silva Emery, *Dyes Pigments.* **2020**, *173*, 107885.

[8] W. Qin, V. Leen, T. Rohand, W. Dehaen, P. Dedecker, M. Van Der Auweraer, K. Robeyns, L. Van Meervelt, D. Beljonne, B. Van Averbeke, J. N. Clifford, K. Driesen, K. Binnemans, N. Boens, *J. Phys. Chem. A* **2009**, *113*, 439–447.

[9] G. Ulrich, R. Ziessel, *J. Org. Chem.* **2004**, *69*, 2070–2083.

[10] S. Xuan, N. Zhao, X. Ke, Z. Zhou, F. R. Fronczek, K. M. Kadish, K. M. Smith, M. G. H. Vicente, *J. Org. Chem.* **2017**, *82*, 2545–2557.

[11] M. Kollmannsberger, T. Gareis, S. Heinl, J. Daub, J. Breu, *Angew. Chemie Int. Ed. English* **1997**, *36*, 1333–1335.

[12] a) V. J. Richards, A. L. Gower, J. E. H. B. Smith, E. S. Davies, D. Lahaye, A. G. Slater, W. Lewis, A. J. Blake, N. R. Champness, D. L. Kays, *Chem. Commun.* **2012**, *48*, 1751–1753; b) A. Kaur, J. L. Kolanowski, E. J. New, *Angew. Chem. Int. Ed. English* **2016**, *55*, 1602-1613.

[13] A. B. Nepomnyashchii, M. Bröring, J. Ahrens, A. J. Bard, *J. Am. Chem. Soc.* **2011**, *133*, 8633–8645.

[14] A. B. Nepomnyashchii, A. J. Bard, *Acc. Chem. Res.* **2012**, *45*, 1844–1853.

[15] R. Y. Lai, A. J. Bard, *J. Phys. Chem. B* **2003**, *107*, 5036–5042.

[16] A. B. Nepomnyashchii, S. Cho, P. J. Rossky, A. J. Bard, *J. Am. Chem. Soc.* **2010**, *132*, 17550–17559.

[17] A. B. Nepomnyashchii, M. Bröring, J. Ahrens, A. J. Bard, *J. Am. Chem. Soc.* **2011**, *133*, 19498–19504.

[18] A. B. Nepomnyashchii, M. Bröring, J. Ahrens, R. Krüger, A. J. Bard, *J. Phys. Chem. C* **2010**, *114*, 14453–14460.

[19] A. B. Nepomnyashchii, A. J. Pistner, A. J. Bard, J. Rosenthal, *J. Phys. Chem. C*

2013, *117*, 5599–5609.

[20] J. Suk, K. M. Omer, T. Bura, R. Ziessel, A. J. Bard, *J. Phys. Chem. C* **2011**, *115*, 15361–15368.

[21] J. E. Dick, A. Poirel, R. Ziessel, A. J. Bard, *Electrochim. Acta* **2015**, *178*, 234–239.

[22] E. A. Leushina, I. A. Usol'Tsev, S. I. Bezzubov, A. A. Moiseeva, M. V. Terenina, A. V. Anisimov, I. V. Taydakov, A. V. Khoroshutin, *Dalt. Trans.* **2017**, *46*, 17093–17100.

[23] Z. Biyiklioglu, T. Keleş, *Inorganica Chim. Acta* **2017**, *466*, 130–138.

[24] O. Hammerich: Reduction of nitro compounds and related substrates. In Organic electrochemistry. Edited by Hammerich O, Speiser B. 5th ed., Taylor & Francis Boca Raton; **2016**: pp. 1181–1182..

[25] D. Beaudoin, J. D. Wuest. *Chem. Rev*. **2016**, *116*, 258–286;

[26] G. Gronchi; P. Courbis; P. Tordo; G. Mousset; J. Simonet, *J. Phys. Chem.* **1983**, *87*, 1343–1349.

[27] T. L. Silva, J. C. S. da Silva, D. J. P. Lima, F. R. Ferreira, C. C. de Vasconcelos, D. C. Santos, C. D. Netto, P. R. R. Costa, M. O. F. Goulart, *J. Braz. Chem. Soc.* **2019**, *30*, 2438–2451.

[28] A. D. Becke, *J. Chem. Phys.* **1993**, *98*, 5648–5652; C. Lee, W. Yang, R. G. Parr, *Phys. Rev. B* **1988**, *37*, 785–789.

[29] S. Grimme, *J. Comput. Chem.* **2006**, *27*, 1787–1799.

[30] R. Ditchfield, W. J. Hehre, J. A. Pople, *J. Chem. Phys.* **1971**, *54*, 720–723.

[31] W. J. Hehre, W. A. Lathan, *J. Chem. Phys.* **1972**, *56*, 5255–5257.

[32] F. De Jong, M. Feldt, J. Feldt, J. N. Harvey, *Phys. Chem. Chem. Phys.* **2018**, *20*, 14537–14544.

[33] J. Tomasi, B. Mennucci, R. Cammi, *Chem. Rev.* **2005**, *105*, 2999–3093.

[34] M. J. Frisch, G. W. Trucks, H. B. Schlegel, G. R. Scuseria, M. A. Robb, J. R. Cheeseman, G. Scalmani, V. Barone, B. Mennucci, G. A. Petersson, H. Nakatsuji, M. Caricato, X. Li, H. P. Hratchian, A. F. Izmaylov, J. Blonio, G. Zheg,

J. L. Sonnenberg, M. Hada, M. Ehara, K. Toyota, R. Fukuda, J. Hasegawa, M. Ishida, T. Nakajima, Y. Honda, O. Kitao, H. Nakai, T. Vreven, J. A. Montgomery, J. E. Peralta, F. Ogliaro, M. Bearpark, J. J. Heyd, E. Brothers, K. N. Kundin, V. N. Staroverov, T. Keith, R. Kobayashi, J. Normand, K. Raghavachari, A. Rendell, J. C. Burant, S. S. Iyengar, J. Tomasi, M. Cossi, N. Rega, J. M. Millam, M. Klene, J. E. Knox, J. B. Cross, V. Bakken, C. Adamo, J. Jaramillo, R. Gomperts, R. E. Stratmann, O. Yazyev, A. J. Austin, R. Cammi, C. Pomelli, J. W. Ochterski, R. L. Martin, K. Morokuma, V. G. Zakrzewski, G. A. Voth, P. Salvador, J. J. Dannenberg, S. Dapprich, A. D. Daniels, O. Farkas, J. B. Foresman, J. V. Ortiz, J. Cioslowski, D. J. Fox, Gaussian09, Revision C.01; Gaussian, Inc., Wallingford, CT, 2013.

[35] T. Lu, F. Chen, *J. Comput. Chem.* **2012**, *33*, 580–592.

[36] K. Krumova, G. Cosa, *J. Am. Chem. Soc.* **2010**, *132*, 17560–17569.

[37] E. Rivera-Gonzalez, E. K. Galvan-Miranda, M. Aguilar-Martínez, N. Farfan, E. Xochitiotzi-Flores, N. A. M. Ruvalcaba. *Electrochim. Acta* **2019**, *317*, 375–383.

[38] C. R. Wilke, P. Chang, *AIChE Journal*, **1955**, *1*, 264.

[39] See, for example, D. R. Lide (ed.), *CRC Handbook of Chemistry and Physics*, 76th edn., CRC Press, Boca Raton, Fl., **1995**.

[40] J. R. Jezorek, H. B. Mark, Jr., *J. Phys. Chem*., **1970**, *74*, 1627–1633.

[41] P.-C. Maria, J.-F. Gal, *J. Phys. Chem.*, **1985**, *89*, 1296–1304.

[42] G. Cauquis, M. Genies, H. Lemaire, A. Rassat, J. P. Ravet, *J. Chem. Phys*. **1967**, *47*, 4642–4644.

[43] L. C. D. Rezende, M. M. Vaidergorn, J. C. B. Moraes, F. S. Emery, *J. Fluoresc.* **2014**, *24*, 257–266.

[44] M. Broring, R. Krüger, S. Link, C. Kleeberg, S. Koehler, X. Xie, B. Ventura, L. Flamigni, *Chem. Eur J.* **2008**, *14,* 2976–2983

[45] N. J. Findlay, C. Orofino-Peña, J. Bruckbauer, S. E. T. Elmasly, S. Arumugam, A. R. Inigo, A. L. Kanibolotsky, R. W. Martin, P. J. Skabara, *J. Mater. Chem. C* **2013**, *1*, 2249–2256.

[46] I. Esnal, J. Banuelos, I. L. Arbeloa, A. Costela, I. Garcia-Moreno, M. Garzón, A. R. Agarrabeitia, M. J. Ortiz, *RSC Adv.*, **2013**, *3*, 1547–1556.

[47] L. J. Núñez-Vergara, J. C. Sturm, C. Olea-Azar, P. Navarrete-Encina, S. Bollo, J. A. Squella, *Free Radic. Res.* **2000**, *32*, 399–409; L. J. Nunez-Vergara, J.A. Squella, C. Olea-Azar, S. Bollo, P.A. Navarrete-Encina c, J.C. Sturm Electrochimica Acta 45 (2000) 3555–3561. *Electrochim. Acta* **2000,** *45,* 3555–3561; L. J. Núñez-Vergara, M. Bonfá, J. C. Sturm, P. Navarrete-Encina, S. Bollo, J. A. Squella, J. Electroanal. Chem. 2001, 506, 48.

[48] I.J. Arroyo-Cordoba, R. Sola-Llano, N. Epelde-Elezcano, I. Arbeloa Lopez, V. Martínez-Martínez, E. Pena-Cabrera, *J. Org. Chem.* **2018,** *83*, 10186e10196.

[49] D. Jacquemin, E. A. Perpète, *Chem. Phys. Lett.* **2006**, *420*, 529–533.

[50] A. Poirel, A. De Nicola, P. Retailleau, R. Ziessel, *J. Org. Chem.* **2012**, *77*, 7512–7525.